

Raman Spectra and Phase Transitions in the Rb 2 KScF 6 Elpasolite

A. S. Krylov , A. N. Vtyurin , A. Bulou & V. N. Voronov

To cite this article: A. S. Krylov , A. N. Vtyurin , A. Bulou & V. N. Voronov (2003) Raman Spectra and Phase Transitions in the Rb 2 KScF 6 Elpasolite, *Ferroelectrics*, 284:1, 47-64, DOI: [10.1080/00150190390204709](https://doi.org/10.1080/00150190390204709)

To link to this article: <https://doi.org/10.1080/00150190390204709>



Published online: 22 Jan 2011.



Submit your article to this journal [↗](#)



Article views: 39



View related articles [↗](#)



Citing articles: 2 View citing articles [↗](#)

Raman Spectra and Phase Transitions in the Rb_2KScF_6 Elpasolite

A. S. KRYLOV,¹ A. N. VTYURIN,^{1,*} A. BULOLO,²
and V. N. VORONOV¹

¹*Kirensky Institute of Physics, Krasnoyarsk, 660036 Russia*

²*Université du Maine, Le Mans, Cedex 9, 72085 France*

(Received June 25, 2002; in final form July 22, 2002)

Raman spectra of Rb_2KScF_6 elpasolite crystal have been studied in a wide temperature range, including two transition points: from cubic to tetragonal, and then—to the monoclinic phase. For the first time both for this crystal and for fluoride elpasolites in general soft modes restoration has been found below transition points; in agreement with selection rules a splitting of degenerate modes has been observed as well both for lattice vibrations and internal modes of ScF_6 octahedrons. Parameters of Raman lines have been quantitatively analyzed and found in good agreement with known thermodynamic characteristics of these transitions; in particular, lines widths are shown to be determined by tree-phonons anharmonic interactions. A wide region of pretransitional fluctuations was found above the upper transition point.

Keywords: Rb_2KScF_6 ; phase transitions; Raman scattering; soft modes

PACS: 63.20.Dj; 63.70.+h; 64.70 Kb; 77.80.Bh; 78.30.-j; 78.30.Hv.

Elpasolites A_2BCX_6 (high symmetry phase G_0 , space group $Fm\bar{3}m$, $Z = 4$, unit cell structure is shown in Fig. 1), are one of the perovskite-like family of crystals that are extensively studied due to their wide variety of structures and excitedly complicated sequences of phase transitions [1]. Their structural phase transitions are usually connected with lattice instability to CX_6 octahedra rotations due to soft phonons condensation. Up to now such lattice modes softening was observed experimentally only in bromine-, chlorine- and oxygen-containing elpasolites (see, e.g., [2–5]). Spectral investigations of fluorine-containing elpasolites are usually complicated because of their higher transition temperatures, and Rb_2KScF_6 crystal seems like giving a good chance for such work. Its transitions temperatures are reasonably low, $T_1 = 252$ K (into G_1 phase, space group $I114/m$, $Z = 2$) and

*Corresponding author. E-mail: vtyurin@iph.krasn.ru

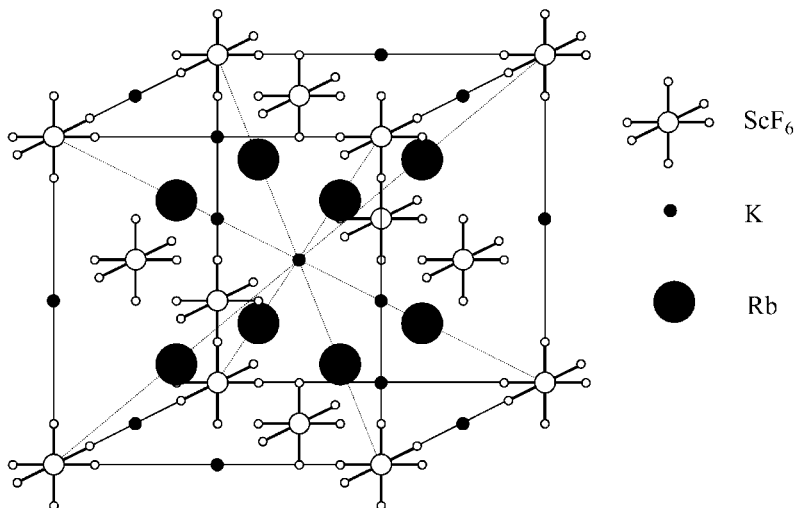


Figure 1. Unit cell structure of Rb_2KScF_6 cubic phase.

$T_2 = 223$ K (into G_2 phase, space group $P12_1/n1$, $Z = 2$) [6], that gives a hope for weaker effects of lattice anharmonicity, not so wide spectral lines and lower background scattering.

Ab initio simulations of lattice stability and dynamics for this crystal have shown [7, 8] that soft mode condensation could induce these phase transformations, but previous experimental Raman scattering studies [9] revealed neither soft mode condensations or restorations no other pretransitional anomalies of vibrational spectra—similar to several other fluorine-containing elpasolites [10].

Therefore we've performed this more detailed investigation of Raman spectra of Rb_2KScF_6 crystal.

Vibrational representation of the cubic phase group at Brillouin zone center is:

$$\Gamma_{\text{vibr}} = A_{1g}(xx, yy, zz) + E_g(xx, yy, zz) + 2F_{2g}(xz, yz, xy) \\ + F_{1g} + 5E_{1u} + F_{2u},$$

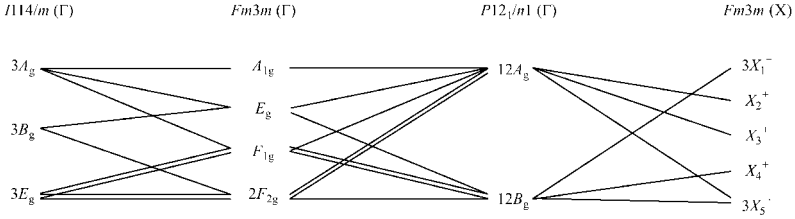
where corresponding components of the Raman scattering tensor are given in brackets. Table shows atoms participating in these vibrations. Site symmetry of ScF_6 ions coincides with the free ion symmetry; symmetry and frequencies of the free ion vibrations are [11]: $\nu_1(A_{1g}) - 498 \text{ cm}^{-1}$, $\nu_2(E_g) - 390 \text{ cm}^{-1}$,

TABLE Vibrational representation for Rb_2KScF_6 cubic phase

ir. rep.	$A_{1g} (xx, yy, zz)$	$E_g (xx, yy, zz)$	F_{1g}	$F_{2g} (xz, yz, xy)$	F_{1u}	F_{2u}
2Rb	–	–	–	1	1	–
K	–	–	–	–	1	–
Sc	–	–	–	–	1	–
6F	1	1	1	1	2	1
Γ_{vibr}	1	1	1	2	5	1

Components of Raman tensor are given in brackets.

Presentation of the cubic–tetragonal soft mode is marked bold.

**Figure 2.** Compatibility relations for Raman active modes of cubic, tetragonal and monoclinic phases of Rb_2KScF_6 .

$\nu_3(F_{1u}) - 176 \text{ cm}^{-1}$, $\nu_4(F_{1u}) - 90 \text{ cm}^{-1}$, $\nu_5(F_{2g}) - 230 \text{ cm}^{-1}$, $\nu_6(F_{2u})$ —frequency unknown. Compatibility relations for Raman active vibrations of cubic and tetragonal phases are presented in Fig. 2. It follows from this diagram that Raman spectrum of the cubic phase includes one hard lattice vibration (the rest are ScF_6 internal modes) while F_{1g} soft mode, if exists, is inactive here; below the first transition it should split into two Raman active lines restoring under further cooling. Splitting of degenerated modes, both internal (E_g and F_{2g}) and lattice (F_{2g}), should appear in G_1 phase as well.

First order transformation to G_2 phase corresponds to X_2^+ irreducible representation of G_0 phase or Z_2^+ of G_1 phase; (we use same notations as in [10]) and doubles unit cell volume. Modes from $X(0, 0, \pi/a)$ point of Brillouin zone are Raman inactive, of course, but as it can be seen in Fig. 2, they should be activated below the second transition point—including restoring of X_2^+ soft mode (if it exists).

Samples for experiments ($2 \times 2 \times 4 \text{ mm}^3$) were taken from the same crystallization as in [6] and cut along crystallographic axes of the cubic phase. They were optically transparent and without colored defects or inclusions visible under the microscope. Back scattering spectra were obtained with T-64000 Raman spectrometer (I.S.A., Jobin Yvon) with nitrogen-cooled

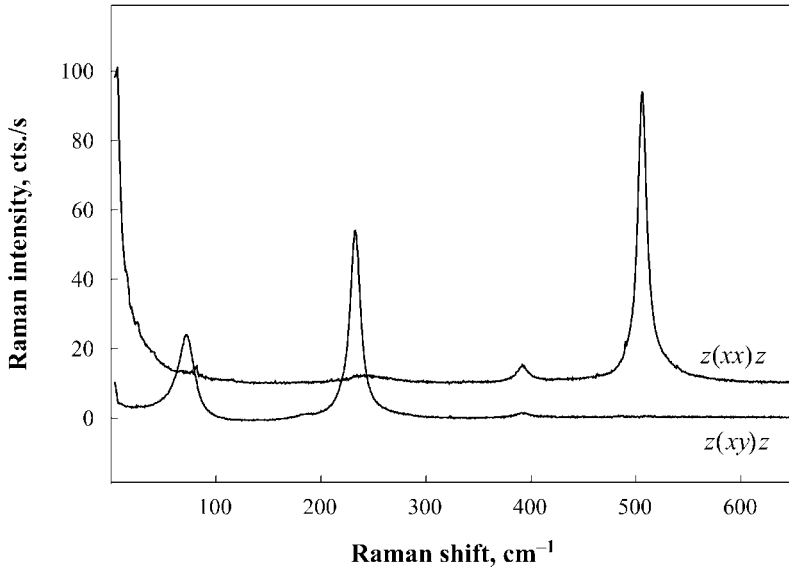


Figure 3. Raman scattering spectra of Rb_2KScF_6 cubic phase ($T = 300$ K).

CCD detector. To reduce low frequency wing of elastic scattering low frequency spectra have been registered in subtractive mode and the lower frequency part of the spectrum was cut at 8 cm^{-1} ; higher frequency internal modes have been taken at maximal resolution, in additive mode. Spectral width of CCD matrix cell was $650/1024\text{ cm}^{-1}$ for subtractive mode and $220/1024\text{ cm}^{-1}$ —for the additive mode one, signal acquisition time —600 c. Spectra were excited with 514.5 nm 500 mW Ar^+ laser line. Temperature stabilization during acquisition was better than 0.2 K .

Number and polarization of the lines observed in the cubic phase far from $G_0 - G_1$ transition point agree well with predicted ones by selection rules and obtained in [9, 10] (Fig. 3). Lines at 505 , 390 and 230 cm^{-1} correspond to internal ScF_6 modes (ν_1 , ν_2 and ν_5 respectively). Frequency of the only Raman active lattice mode is 89 cm^{-1} at room temperature. It should be pointed out that phase transition gives rise to formation of complicated domain structure that, in addition to birefringence effects, prevents observations of polarized spectra below transition point.

Transformation of the lower frequency part of the spectrum (that corresponds to lattice vibrations) is given in Fig. 4. It could be subdivided into two parts: below and above 60 cm^{-1} . Higher frequency part includes hard lattice modes. Here we observe slow high frequency shift of 89 cm^{-1} lattice

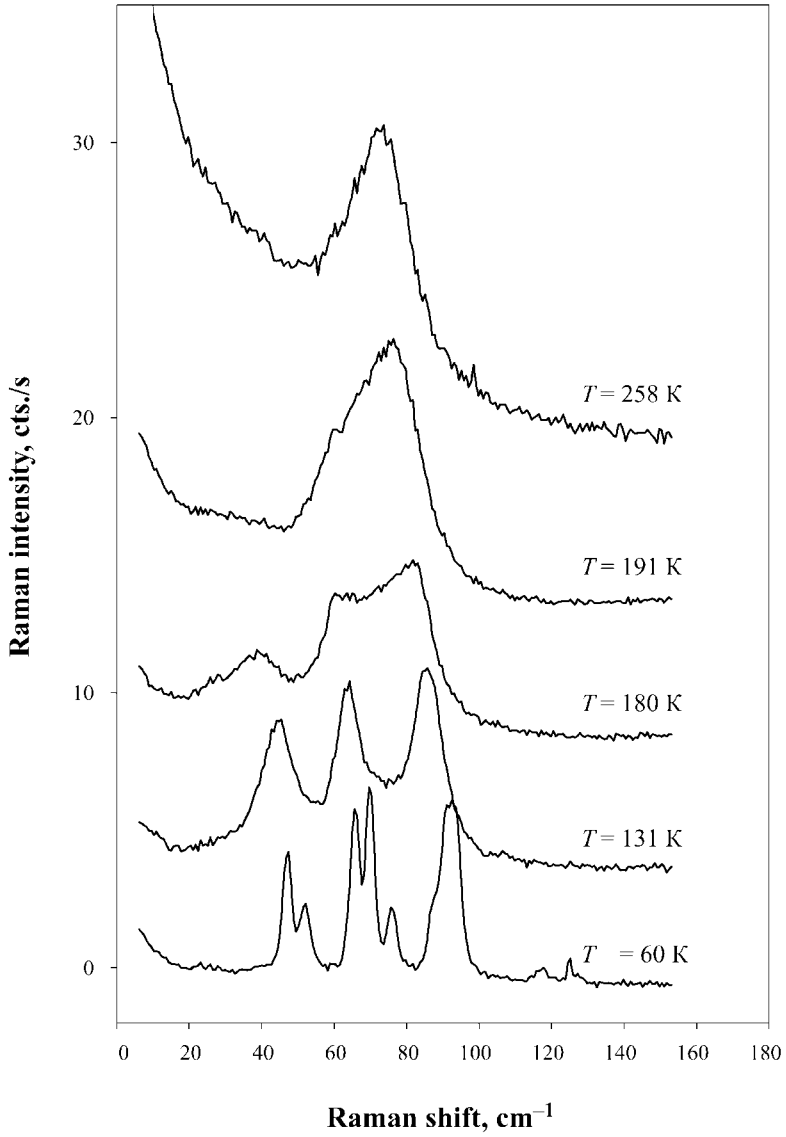


Figure 4. Temperature transformation of low frequency lattice modes spectrum.

mode mentioned above, that splits in two below T_1 transition point; next transition at T_2 results in its further splitting and deeper cooling gives rise for extra weaker lines appearance. Temperature dependences of these positions and widths, as well as their compatibility relations are given in Fig. 5. As it is clearly seen from the figure, total number of the lines observed in this spectral region corresponds to crystal symmetry perfectly.

It's interesting to point out that splitting of degenerate lines shows off just below transition points, while extra lines induced by unit cell doubling appear far below $G_1 - G_2$ transition.

In the lowest ($<60 \text{ cm}^{-1}$) part of the spectra we've observed growth and widening of the central peak wing under cooling just above the upper transition point. Below T_1 this wide wing may be interpreted as an appearance of a low frequency weak wide band point (Fig. 4), where two maxima (at 26 cm^{-1} and 39 cm^{-1}) may be marked out closer to T_2 temperature. Figure 6 demonstrates temperature dependences of these maxima positions. Parameters of these overlapped lines have been determined with SigmaPlot 5.0 package (SPSS Inc.) using dispersion line contours, with preliminary correction of intensity distribution for temperature drift of vibrational states populations:

$$I_s(\Omega_\alpha) \sim |Q_\alpha|^2 \sim n_\alpha + 1 = \frac{1}{1 - \exp(-\hbar\Omega_\alpha/k_B T)}$$

We did not find any definite shift of these lines' position within tetragonal phase (though precision of the deconvolution procedure here was not too high due to intense noise of background scattering); we can only point out some «intensity transfer» to higher frequency wing of this band on cooling.

Intensity of this higher frequency component grows stepwise at the second transition point. It's position starts to drift up, and squared frequency grows about linearly with temperature going further down. Such linear temperature dependence is typical for soft modes at phase transitions of the second order or of the first one, close to second. Line widths drop continuously and below 100 K this upper line splitting into doublet becomes visible. Upper component of this doublet moves continuously further under cooling, while lower one stays practically on the spot ($47\text{--}48 \text{ cm}^{-1}$).

Position of the lowest maximum ($23\text{--}27 \text{ cm}^{-1}$) stays about constant under cooling as well. It's intensity decreases slowly, and below 100 K it can be hardly seen above background level.

These results are in good agreement with selection rules for the soft modes of studied phase transitions (see compatibility relations at Fig. 6(b)).

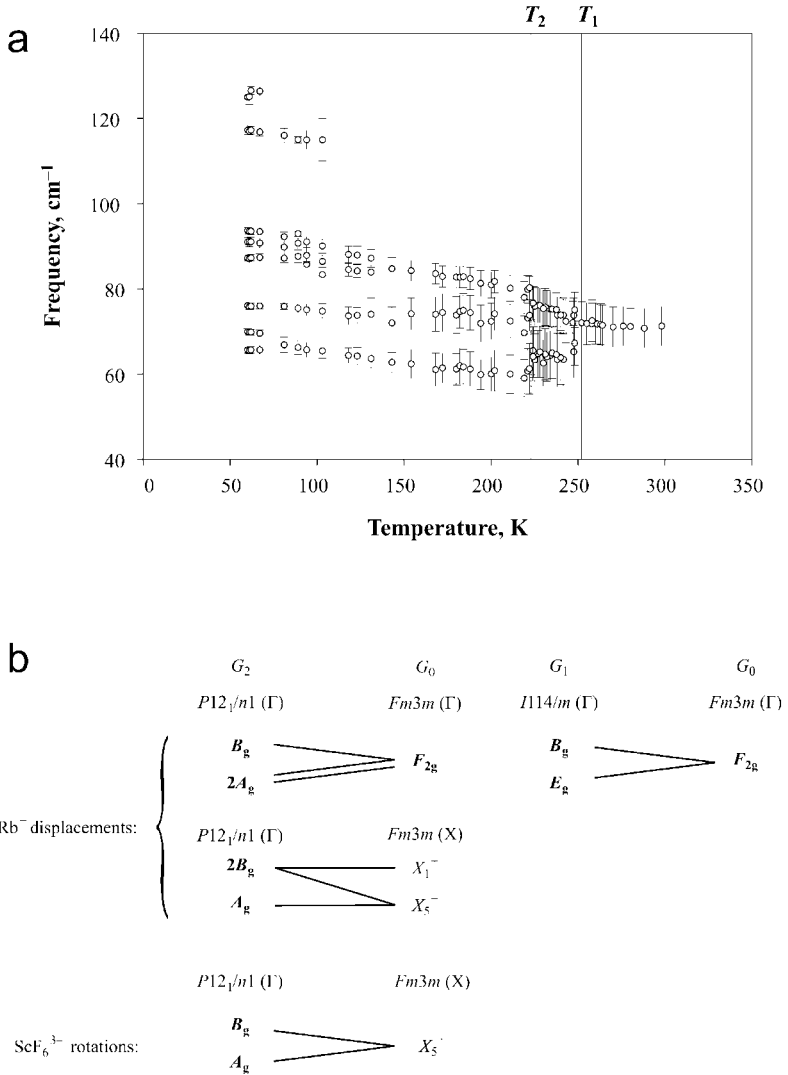


Figure 5. Temperature dependences of hard lattice modes positions (a), vertical bars—their widths (HWHH); and (b)—their compatibility relations, Raman active modes are marked bold.

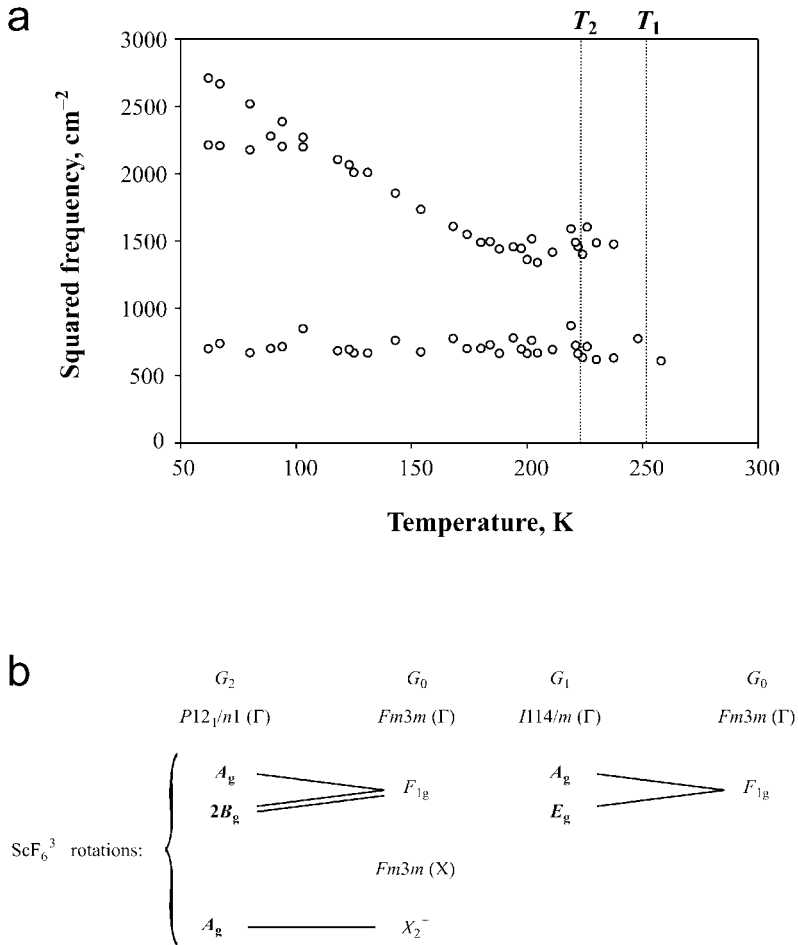


Figure 6. Temperature dependence of squared frequencies of lower frequency lattice modes (a) and their compatibility relations (b).

According to this diagram, two modes should restore below T_1 after condensation and partial splitting of F_{1g} soft mode, Raman inactive in G_0 phase. After the second transition they should split further forming a triplet ($A_g + 2B_g$). Besides one more mode, soft mode of this transition, should restore here, of A_g symmetry in the lower temperature phase. It's interaction with A_g component of the triplet will move both of them up—until their repulsion. Two other B_g components of the triplet could

stay at the place (within normal temperature dependence). It's interesting to point out that *ab initio* lattice dynamics simulation of G_2 phase at $T = 0$ [7] gives two lowest frequencies equal to 21 and 26.6 cm^{-1} , that agrees perfectly with the position of our lower frequency maximum (23–27 cm^{-1}).

According to selection rules both soft modes in higher symmetry phases correspond to ScF_6 groups' rotations without their distortions or admixing of other degrees of freedom—there are no other vibrations of the same symmetry in the crystals spectrum. However below transition symmetry allows for such interaction with rubidium ions displacements, that could be mixed up to eigenvectors of restoring modes.

Besides lattice modes, we've studied high resolution (effective spectral slit width 0.2 cm^{-1}) spectra of ScF_6 groups internal modes. Temperature evolution of these spectra in the region of F_{2g} mode is given in Fig. 7. Figures 8 and 9 show temperature dependences of observed lines' positions and of the width of the strongest line.

Number of lines, observed here, agrees with selection rules for these phases (compatibility relations for ScF_6 internal modes are presented in Fig. 8(b)). Position of the strongest line stays practically constant (232 cm^{-1}) within whole studied temperature range of the cubic phase, that supposes compensation of the effects of temperature expansion and phonon-phonon interactions on phonon frequency. Below the cubic to tetragonal phase transition line frequency changes continuously and it splits into doublet. At the second transition these frequencies changes stepwise and they split further. Continuous transformation at the upper transition and stepwise—at the second one agree with thermodynamic data [6] on these transitions. Again, as it has been observed for lattice modes, lines that come from Brillouin zone boundary, are of very weak intensity and appear above background level far below transition temperature.

Approximation of the line 232 cm^{-1} damping constant with dependence:

$$\sigma(\Omega_\alpha, T) = \sigma(\Omega_\alpha, 0) \left(1 + \frac{1}{\exp(\hbar\Omega_{\beta 1}/k_B T) - 1} + \frac{1}{\exp(\hbar\Omega_{\beta 2}/k_B T) - 1} \right),$$

that corresponds to decay into two phonons [12], gives zero temperature width of 0.1 cm^{-1} and participating phonon frequency of 224 cm^{-1} , and is consistent with phonon splitting into one optic and another acoustic phonons from Brillouin zone boundary. Some anomalies of the phonon damping are clearly seen near phase transitions, that may be connected with its interaction with order parameter fluctuations.

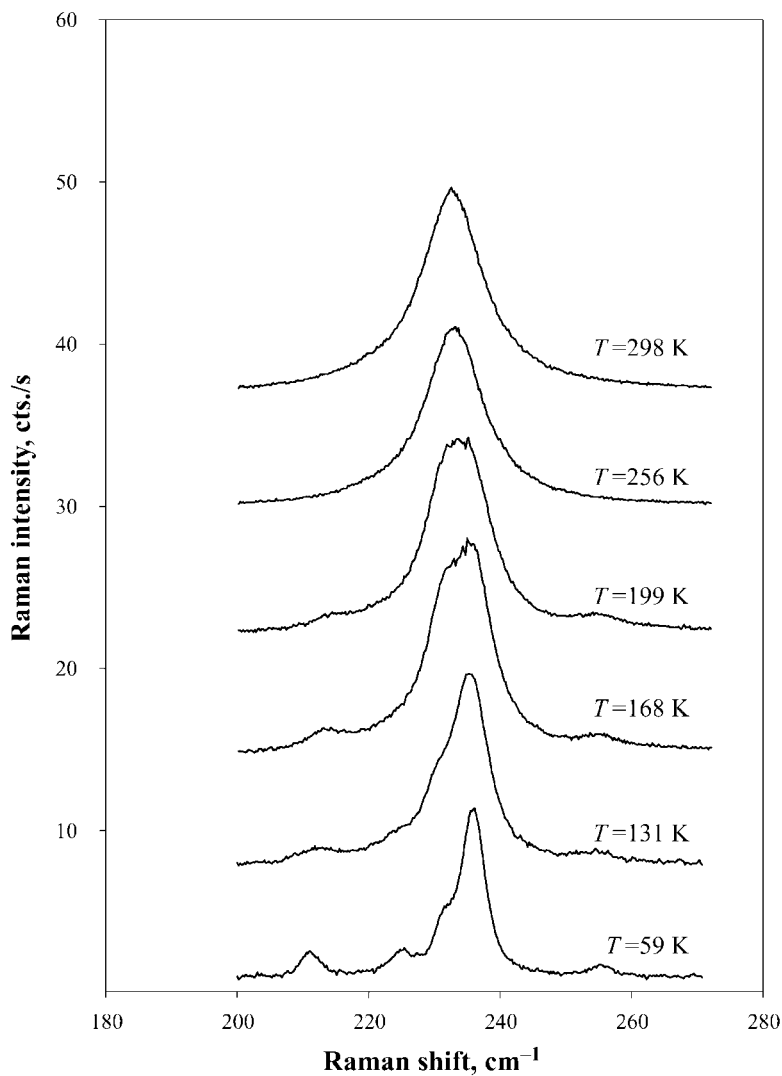


Figure 7. Temperature transformation of the spectrum near ν_5 (F_{2g}) internal mode.

The line, corresponding to ν_2 internal mode, is the weakest one in the spectrum (see Fig. 3), so we failed to observe its splitting below transition points. Temperature dependence of its position is shown at Fig. 10. This dependence changes abruptly at the upper transition point: nearly constant

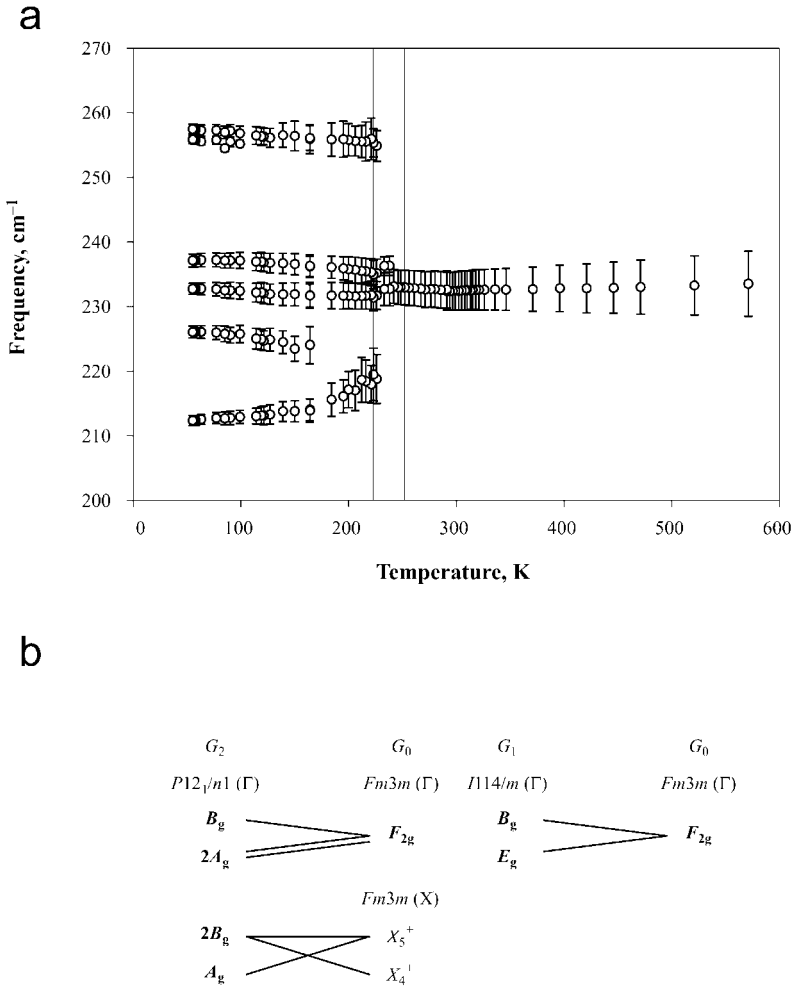


Figure 8. Temperature dependence of ν_5 internal modes positions (a) and their compatibility relations (b). Raman active modes are marked bold.

at the lower phases the frequency goes down continuously under heating in the cubic phase. Extrapolation of this dependence in the cubic phase with the function [12, 13]:

$$\Omega_\alpha(T) = \Omega_\alpha(0) \exp(-3\gamma_\alpha aT),$$

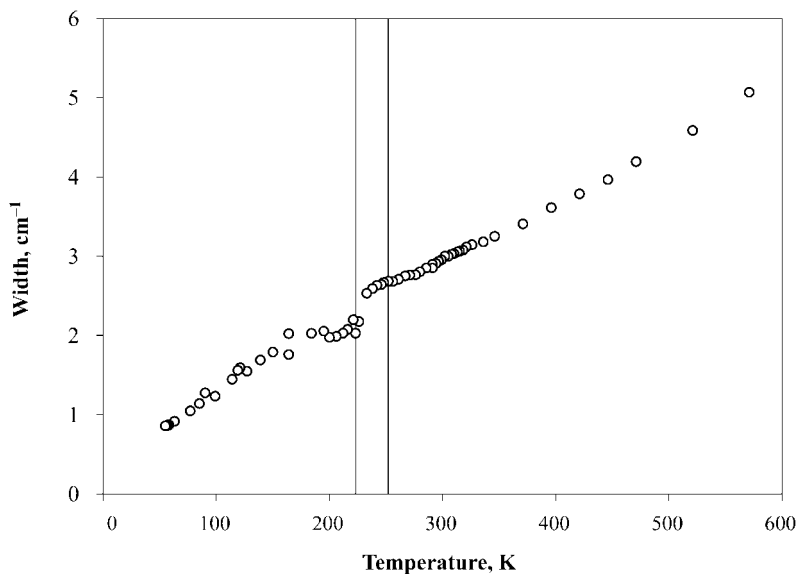


Figure 9. Temperature dependence of the width (HWHH) for the most intensive ν_5 internal mode.

gives product of Grunizen parameter by temperature expansion coefficient $\gamma_\alpha a \approx 0.4 \times 10^{-4} \text{ K}^{-1}$; extrapolated to $T = 0$ frequency value is 407 cm^{-1} .

Close positions of ν_1 and ν_2 lines provides a possibility to get them in one high resolution spectrum and to measure their relative intensity (it was mentioned above that domain structure of lower phases makes such measurements quite difficult). The result is shown in Fig. 11: considerable growth of this intensity is observed around upper transition point.

Temperature evolution of ν_1 internal mode is shown in Fig. 12. New line appearance is clearly seen at lower temperature, that agrees with selection rules (see compatibility relations in Fig. 13(b)). As before, this line coming from Brillouin zone boundary becomes visible somewhere below transition point. Temperature dependences of the positions of these lines is given in Fig. 13. Extrapolated values $\gamma_\alpha a \approx 0.2 \times 10^{-5} \text{ K}^{-1}$ with $T = 0$ frequency equals 518 cm^{-1} . Obtained value of Grunizen parameter, an order less as compared with E_g mode, shows extremely weak anharmonicity of this vibration.

Transition to the tetragonal phase changes considerably temperature dependence of this mode as well (frequency shift from the dependence, extrapolated in the cubic phase, is shown in Fig. 14). Slight deviation from

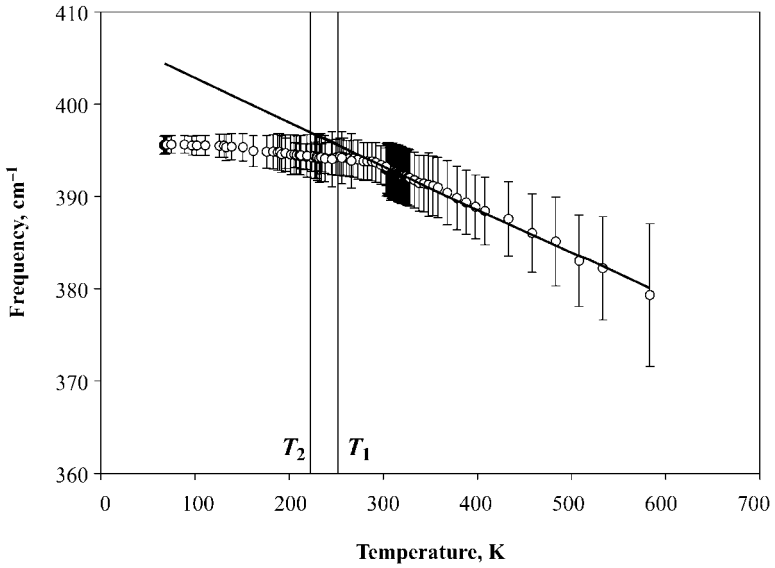


Figure 10. Temperature dependence of ν_2 (E_g) internal mode position. Vertical bars—its width (HWHH), line—extrapolation of cubic phase data.

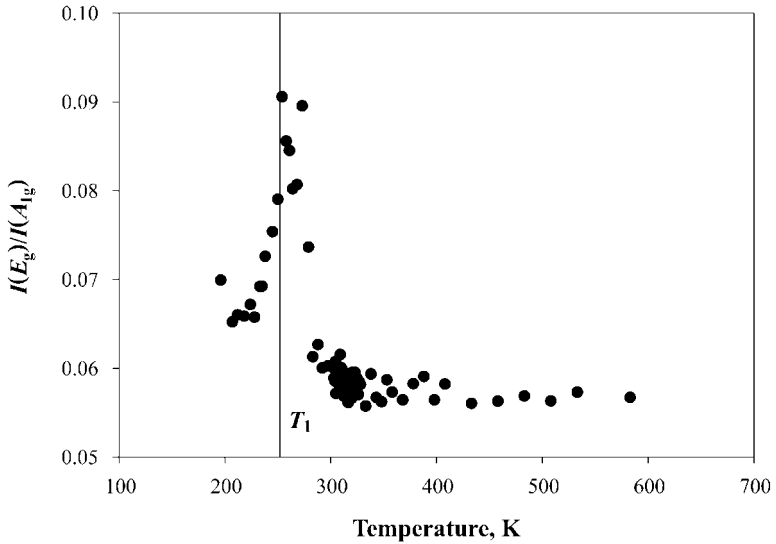


Figure 11. Relative intensity of ν_2 (E_g) internal mode vs. temperature.

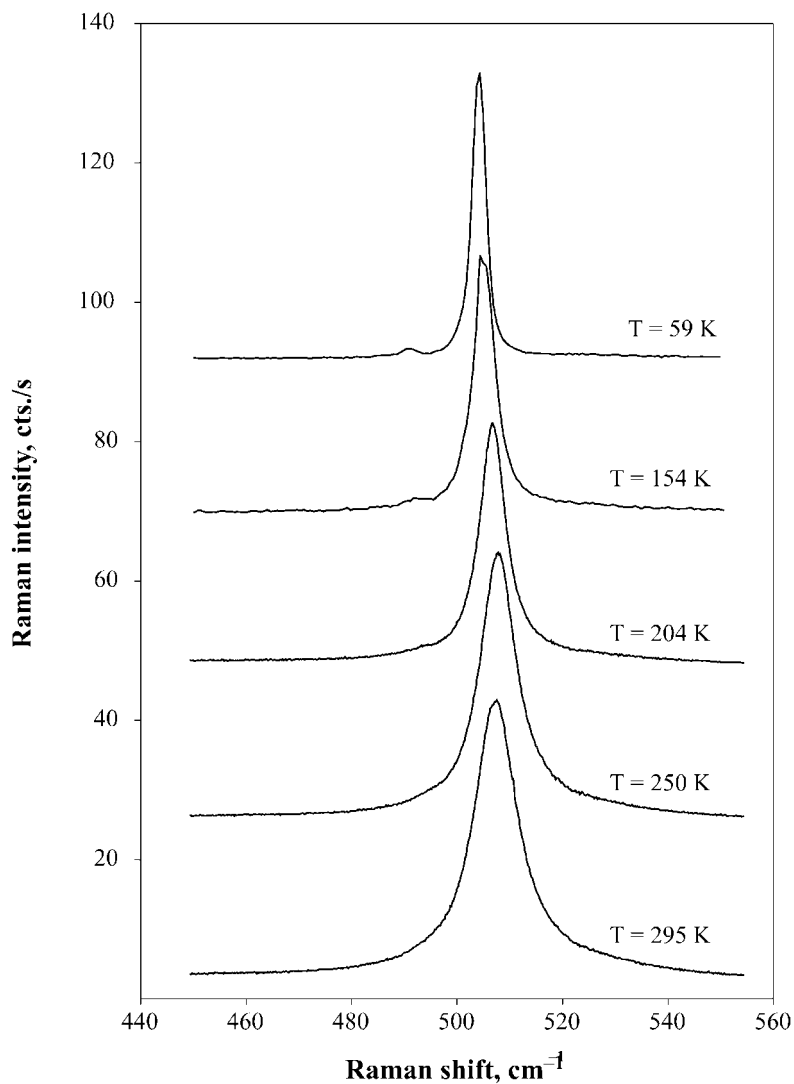


Figure 12. Temperature transformation of the spectrum near $\nu_1 (A_{1g})$ internal mode.

extrapolated value appears even in the cubic phase, in rather wide (about 50 K) pretransitional region. This deviation grows in tetragonal phase and increases linearly with temperature in the monoclinic one, that correspond to the phase transition of the second order or close to second order. Temperature

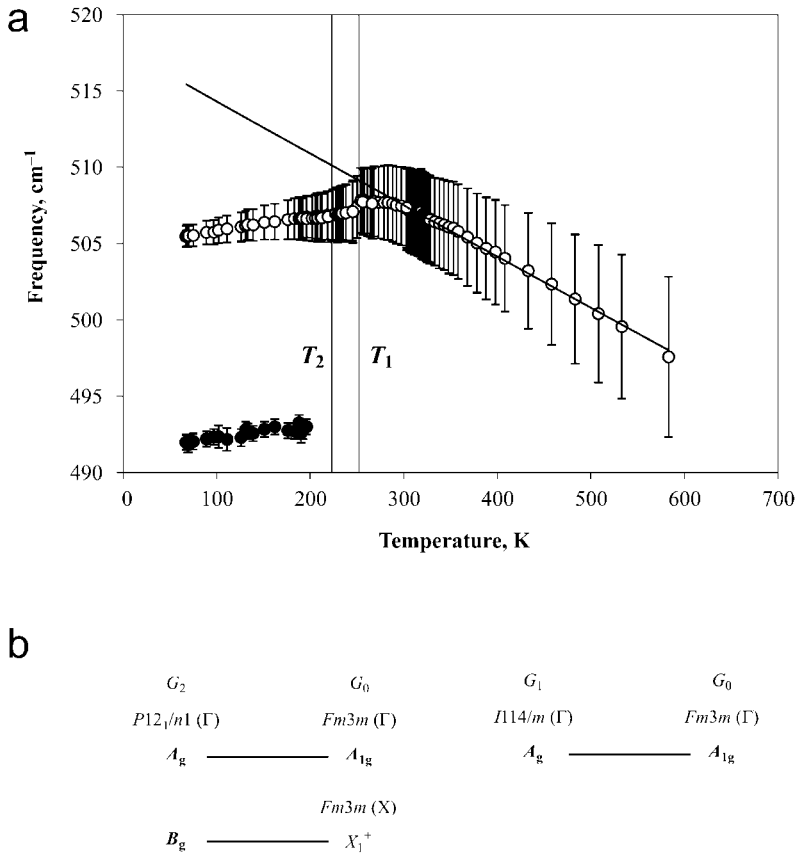


Figure 13. Temperature dependence of $\nu_1 (A_{1g})$ internal modes' positions (a); vertical bars—their widths (HWHH), line—extrapolation of cubic phase data. (b)—their compatibility relations; Raman active modes are marked bold.

region of pretransitional effects agrees well with the one observed by intensity measurements for ν_2 mode (Fig. 11).

Width of this line reveals some transitional effects as well. Its temperature dependence is given in Fig. 15; a curve at the figure is extrapolation of the values for cubic phase. Obtained frequency of the phonon, participating in the decay of this mode, is equal 413 cm^{-1} , that corresponds to the decay into ν_2 internal mode and hard lattice phonon.

Appearance of a weaker line near a stronger one gives a good possibility to compare their intensities—result is given in Fig. 16. In spite of considerable

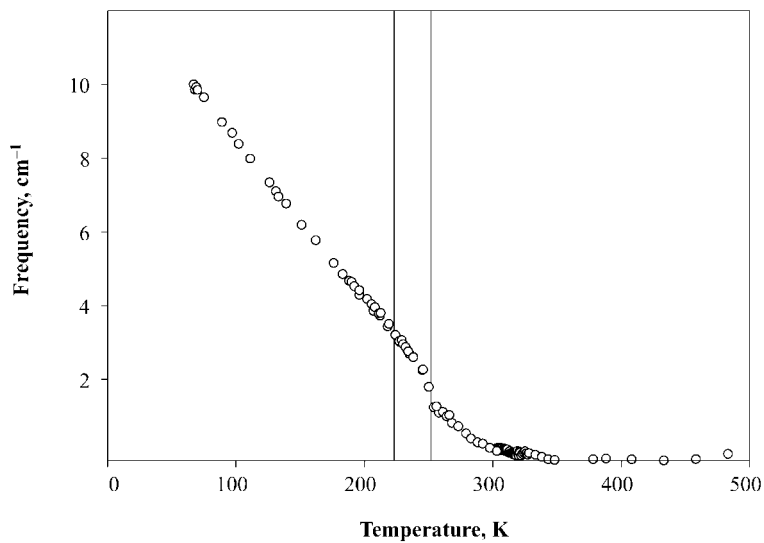


Figure 14. Temperature dependence of ν_1 (A_{1g}) internal mode shift from its extrapolated value.

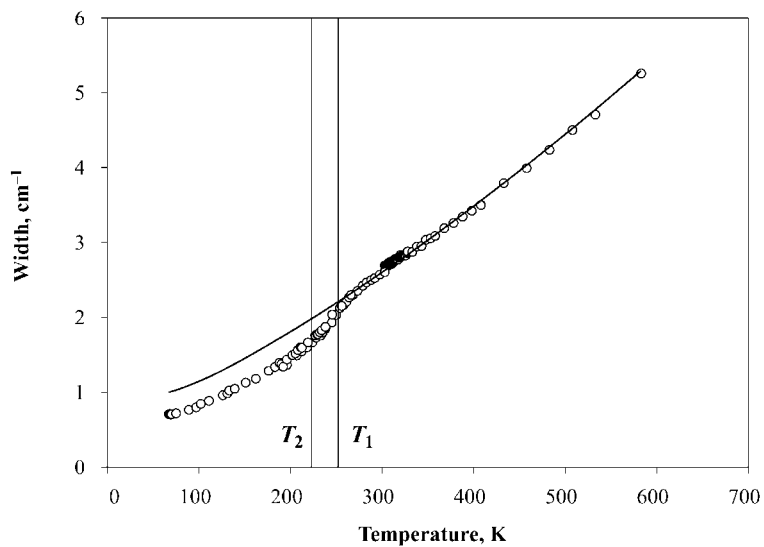


Figure 15. Temperature dependence of the width (HWHH) for the most intensive ν_1 (A_{1g}) internal mode.

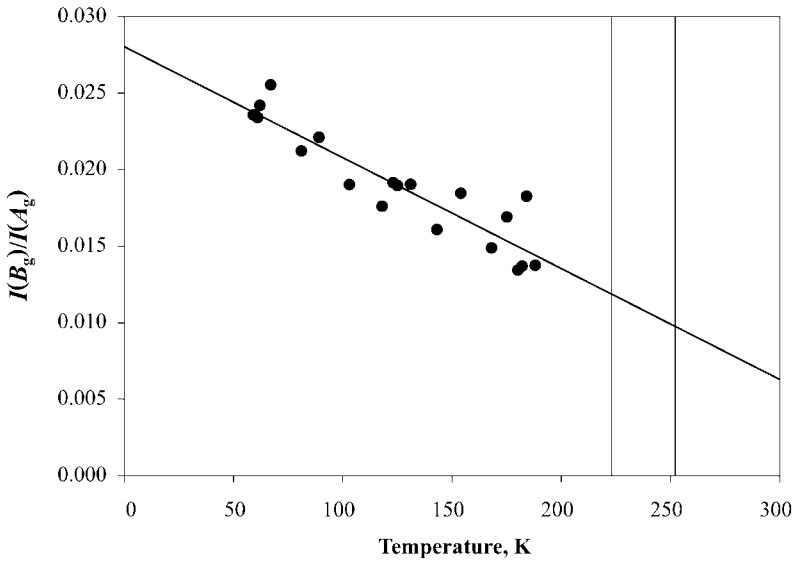


Figure 16. Relative intensity of ν_1 (A_{1g}) doublet components. Line—linear regression.

data scattering (that could be connected with effects of crystal domain structure) one can see, that intensity of the new component of this doublet grows about linearly under cooling. Linear regression line does not come to the transition point, that is typical for first order transitions and agrees with the data [6] for cubic-tetragonal transition.

As a result of these investigations we can conclude, that phase transitions in Rb_2KScF_6 crystals are accompanied with soft modes restorations; that attributes them to displacive phase transitions [8, 9]. According to group theory analysis eigenvectors of both soft modes are connected with rotations of ScF_6^+ ions, though below $G_1 - G_2$ transition these modes could be mixed with other degrees of freedom—in particular, with rubidium ions displacements. Anomalous dependences of parameters of hard lattice and internal modes have been found and interpreted; their quantitative analysis confirms attribution of $G_0 - G_1$ transition to the second order, and $G_1 - G_2$ one—to the first one, close to second. Small values of lines' widths and their temperature dependences confirm that phonon damping in the higher symmetry phase is connected with phonon decays due to their anharmonicity but not to some lattice disordering, with only possible exception for pretransitional region.

ACKNOWLEDGEMENTS

Authors wish to thank Prof. K. S. Aleksandrov, Prof. I. N. Flerov and Prof. V. I. Zinenko for their valuable support and useful discussions. This work has been financially supported by grants INTAS 97-10177, Russian Foundation for Basic Research 00-02-17792 and 02-02-97707.

REFERENCES

- [1] K. S. Aleksandrov and B. V. Beznosikov, *Perovskite-Like Crystals* (Nauka Publishers, Novosibirsk, 1997) (in Russian).
- [2] W. Buhner and H. U. J. Gudel, *Phys. C* **20**, 3809 (1987).
- [3] G. P. Knudsen, *Solid State Commun.* **49**, 1045 (1984).
- [4] F. Prokert and K. Aleksandrov, *Phys. Status Solidi* **b124**, 503 (1984).
- [5] G. Baldinozzi, Ph. Sciau, and A. Bulou, *J. Phys. Condens. Matter.* **7**, 8109 (1995).
- [6] I. N. Flerov, M. V. Gorev, S. V. Melnikova, S. V. Misyul, V. N. Voronov, and K. S. Aleksandrov, *Phys. Solid State* **34**, 2185 (1992).
- [7] V. I. Zinenko and N. G. Zamkova, *Phys. Solid State* **41**, 1297 (1999).
- [8] V. I. Zinenko and N. G. Zamkova, *J. Exper. Theor. Phys.* **118**, 359 (2000).
- [9] I. N. Flerov, M. V. Gorev, K. S. Aleksandrov, A. Tressaud, J. Grannec, and M. Cousi, *Mater. Sci. Eng.* **R24**, 79 (1998).
- [10] M. Cousi, S. Khairoun, and A. Tressaud, *Phys. Stat. Sol.* **a98**, 423 (1986).
- [11] K. Nakamoto, *Infrared and Raman Spectra of Inorganic and Coordination Compounds* (Wiley, New York etc., 1991).
- [12] M. Balkanski, R. F. Wallis, and E. Haro, *Phys. Rev.* **B28**, 1928 (1983).
- [13] J. Gonzalez, E. Moya, and J. C. Chervin, *Phys. Rev.* **B54**, 4707 (1996).